Suppression of turbulence at low power input in a model for plasma confinement transitions

R. Ball

Citation: Physics of Plasmas **12**, 090904 (2005); doi: 10.1063/1.2034327
View online: http://dx.doi.org/10.1063/1.2034327
View Table of Contents: http://scitation.aip.org/content/aip/journal/pop/12/9?ver=pdfcov
Published by the AIP Publishing

Suppression of turbulence at low power input in a model for plasma confinement transitions

R. Ball[a)]
Department of Theoretical Physics, Research School of Physical Sciences and Engineering, The Australian National University, Canberra ACT 0200 Australia

(Received 21 March 2005; accepted 6 July 2005; published online 21 September 2005)

A physics-based condition is used to unfold a trapped or persistent degenerate singularity in a dynamical model for plasma confinement transitions. The bifurcation structure of the resulting enhanced model indicates that shear flow can actually grow as the power input is withdrawn, with concomitant supersuppression of turbulence. This is an important and testable prediction that suggests new design, management, and optimization strategies for new-generation fusion experiments. © *2005 American Institute of Physics*. [DOI: 10.1063/1.2034327]

I. INTRODUCTION

In this work the singularity and bifurcation structures of a model for the coupled dynamics of potential energy, turbulence kinetic energy, and shear flow subsystems in confined fusion plasmas are analyzed. It is found that two hysteresis regimes are possible, one of which allows substantial growth of shear flow and greatly enhanced turbulence suppression as the power input is withdrawn, before the back transition occurs at relatively low power input.

In driven-dissipative flows where Lagrangian fluid elements see a local two-dimensional velocity field the kinetic energy of small-scale turbulent fluctuations can drive the formation of large-scale, stable, coherent structures such as shear and zonal flows. This striking tendency to self-organize is a consequence of local inverse energy cascades.[1] The distinctive properties of quasi-two-dimensional fluid motion are the basis of natural phenomena such as zonal and coherent structurings of planetary flows, but are underexploited in technology.

In magnetically contained fusion plasmas the most potentially useful effect of two-dimensional fluid motion is suppression of high wave-number turbulence that generates anomalous cross-field transport fluxes and degrades confinement,[2] which can manifest as a dramatic enhancement of sheared poloidal or zonal flows and concomitant reduction in turbulent transport. These low- to high-confinement (*L-H*) transitions have been the subject of intensive experimental, *in numero*, theoretical, and modeling investigations since the 1980s.

The extended modeling and analysis in this work are based on the following reduced dynamical model for confinement transitions from Ref. 3:

$$\varepsilon \frac{dP}{dt} = Q - \gamma NP, \tag{1}$$

$$\frac{dN}{dt} = \gamma NP - \alpha v'^2 N - \beta N^2, \tag{2}$$

$$2\frac{dv'}{dt} = \alpha v' N - \mu(P,N)v' + \varphi, \tag{3}$$

where P is the energy in the pressure gradient reservoir, N is the kinetic energy of the turbulence, and $F = \pm v'^2$ is the shear flow kinetic energy. The power input Q is assumed constant, ε is the thermal capacitance, γ and α are the conservative energy-transfer rate coefficients, β is the turbulence dissipation rate coefficient, φ is a shear flow source rate, and $\mu(P,N) = bP^{-3/2} + aPN$ represents the neoclassical and turbulent contributions to viscous dissipation.

Equations (1)–(3) are derived from the following reduced magnetohydrodynamics (MHD) fluid equations for momentum and pressure convection:

$$\rho \frac{d\mathbf{v}}{dt} = -\nabla p + \mathbf{J} \times \mathbf{B} + \mu \nabla_\perp^2 \mathbf{v} + \Omega' \tilde{p}\hat{x} - \rho\nu[\mathbf{v} - V(x)\hat{y}], \tag{4}$$

$$\frac{dp}{dt} = \chi \nabla_\perp^2 p, \tag{5}$$

where $d/dt = \partial/\partial t + \mathbf{v}\cdot\nabla$, together with the incompressibility condition $\nabla\cdot\mathbf{v} = 0$ and the resistive Ohm's law $\mathbf{E} + \mathbf{v} \times \mathbf{B} = \eta\mathbf{J}$. The symbols and notation are defined in Appendix A. Equations (4) and (5) are the electrostatic limit of the reduced MHD equations that were originally derived in Ref. 4. They have been shown to describe well the nonlinear dynamics of a high beta, large aspect ratio, tokamak plasma.[5–8] Here an additional term in the momentum balance has been included, $\rho\nu[\mathbf{v} - V(x)\hat{y}]$, which breaks shear flow reversal symmetry. Averaged energy integrals over slab geometry and semiempirical closure yield Eqs. (1)–(3). (See the Appendix of Ref. 3 for details of the derivation.)

It is helpful to schematize the energy pathways through the potential energy, turbulent kinetic energy, and shear flow subsystems as in Fig. 1. It can be seen that the skeleton of the dynamical system can also be written down directly by inspection, then fleshed out into Eqs. (1)–(3) by using the semiempirical rate expressions that were derived in Refs. 9 and 3.

[a)]Electronic mail: Rowena.Ball@anu.edu.au

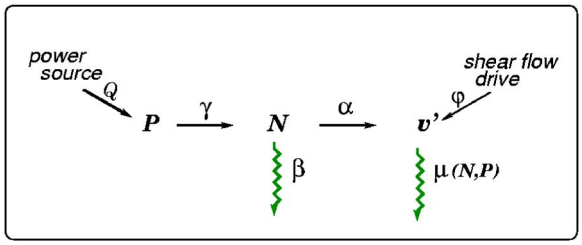

FIG. 1. Energy flux schematic for the gradient-driven plasma turbulence-shear flow system expressed by Eqs. (1)–(3). The curly arrows indicate the dissipative channels, the straight arrows indicate the inputs to and transfer channels between the energy-containing subsystems.

The bifurcation structure of Eqs. (1)–(3) was found in Ref. 3 to predict shear flow suppresion of turbulence, hysteretic, nonhysteretic, and oscillatory transitions, and saturation then decline of the shear flow with increasing power input. All of these behaviors have been observed repeatably in diverse fusion plasma experiments. The model would therefore seem to be a "good" and "complete" one, in the sense of being self-consistent, free of pathological or persistent degenerate singularities, and reflecting typical observed behaviors.

However, a review of the known bifurcation structure in Sec. II identifies a trapped (or persistent) degenerate singular point at zero power input Q and nonzero shear flow input φ, that was not found in the previous work. We label this point as s4. The presence of s4 leads to a breakdown of the model under certain circumstances: from a high-confinement state the equilibrium structure of Eqs. (1)–(3) predicts unbounded growth of the shear flow as the power input Q is withdrawn to zero. The trapped singularity s4 is dissolved (or unfolded) smoothly by introducing a simple lumped model for energy flux from the shear flow to the turbulence. In physical terms the presence of s4 reflects the fact that Eqs. (4) and (5), from which Eqs. (1)–(3) were derived, describe the physics of a flow under a purely two-dimensional velocity field—which, of course, can exist only in simulation. The unfolding of s4 can be viewed as a simple model for the effects of the three-dimensional velocity field that in real life is experienced by the fluid elements, namely, a non-negligible energy cascade to high wave numbers. In terms of the model itself, s4 and the new term that unfolds it highlight the importance of unphysical or trivial solutions in shaping the structure of the physical parameter space. In Sec. III some practical consequences of the unfolding for experiment design and device operation are discussed. The results are summarized in Sec. IV.

A brief exposition on singularity theory and descriptive terminology such as persistent, degenerate, and unfolding, in the current context, is given in Appendix B. Singularity theory is a systematic methodology for characterizing the equilibria of dynamical systems, that involves perturbing around high-order singularities to map the bifurcation landscape. It has been applied in modeling plasma dynamics in Ref. 10. In a broad sense this paper is about using the singularity theory as a diagnostic tool to probe the relationship between the bifurcation structure of the model and the physics of the process it is supposed to represent, in order to compound an impasto picture of confinement transition dynamics. In doing so, we shall take a guided walking tour of Eqs. (1)–(3) and a physics-based extended model, Eqs. (1), (6), and (7), to study the stability of attractors, interrogate degenerate or pathological singularities where they appear, and compute and present selected key bifurcation diagrams.

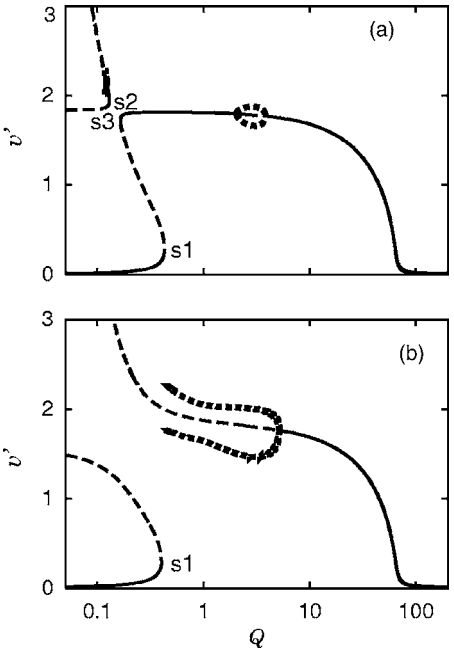

FIG. 2. Representative bifurcation diagrams for Eqs. (1)–(3), illustrating (a) a classical hysteretic transition, for $\varphi=0.08$, and (b) an oscillatory transition, for $\varphi=0.11$. Other parameters $\beta=1$, $\gamma=1$, $b=1$, $a=0.3$, $\alpha=2.4$, and $\varepsilon=1$.

II. THE CASE OF THE TRAPPED SINGULARITY

Two representative bifurcation diagrams for Eqs. (1)–(3) are given in Fig. 2, where the power input Q is the principal bifurcation parameter and the shear flow v', in the positive domain, is chosen as the state variable. (In these and subsequent diagrams the solid lines mark the stable equilibria, the dashed lines mark the unstable equilibria, and the amplitude envelopes of limit cycles are indicated by the solid dots.) A bifurcation diagram may be viewed conceptually as the data plot from a series of experiments. We may imagine conducting an experiment in which we make a small increment in the power input Q, allow the system to evolve to quasiequilibrium, and record the potential energy, turbulence energy, and shear flow (or correlated quantities). This gives us one point on the diagram. We repeat the experiment many times, each time increasing Q by a small amount, and plot the resulting data set. In the limit the increments in Q become quasistatic and we have a continuous bifurcation diagram. We then carry out another set of experiments in which Q is *decreased* quasistatically, to test for and map possible hysteresis. The bifurcation parameter is often referred to as the control parameter. In principle, if not always in practice, it is an external dial or lever that can be twiddled independently by the experimenter during or between experiments. The bifurcation diagrams in Fig. 2 are computed and plotted for

different values of the symmetry-breaking shear flow driving parameter φ. They are rich with information that speaks of some of the known and predicted dynamics of the system. Three features, in particular, should be noted.

- The transition to a high shear flow, or high confinement, state occurs at the turning point labeled as s1 in both (a) and (b).
- In (a) the back transition occurs from a quiescent state at s2. On this high-confinement branch there are two Hopf bifurcations bracketing an enclave of stable limit cycles. The separate branch at high v' and low Q has a turning point labeled as s3 and a Hopf bifurcation from which emanates a small strip of limit cycles, barely discernible at this resolution.
- In (b), where the shear flow drive φ is somewhat stronger, the two separate branches of equilibria have exchanged arms (through a transcritical bifurcation, for details see Ref. 3) and two of the Hopf bifurcations have annihilated each other, through a degenerate point where the pure imaginary eigenvalues pass through zero (a double zero eigenvalue, or DZE). The system transits at s1 to an ocillatory rather than a quiescent high shear flow state. There is no classical hysteresis (i.e., S-shaped cubic normal form) in this region of parameter space: the back transition takes place at the terminus of the limit cycle branch. Near this terminus there is three-dimensional periodic behavior, such as period doubling and wobbling of a limit cycle to a torus, so complex oscillations would be expected.

A. An unphysical prediction

Before I pinpoint the pathology that still exists in this bifurcation structure, it is illuminating to evince the physical—or unphysical—situation by considering Eqs. (1)–(3) on the stretched (or shrunken) time scale $\tau=t/\varepsilon$. In a system of low thermal capacitance $\varepsilon \ll 1$ and $N \approx N_0$ and $v' \approx v_0$. Thus the dynamics becomes quasi-one-dimensional: the potential-energy subsystem sees the kinetic-energy subsystems as nearly constant, and $P \approx [P_0 - Q/(N_0\gamma)] \times \exp(-N_0\gamma\tau) + Q/(N_0\gamma)$. Reverting to real time, as $\varepsilon dP/dt \to 0$ we have $P \approx Q/(\gamma N)$; the potential energy is reciprocally slaved to the kinetic-energy dynamics.

The anomaly in this low-capacitance picture is that, as the power input Q ebbs toward zero, the shear flow can grow quite unrealistically. It is conjectured that the remaining Hopf bifurcation in Fig. 2(b) is captured by a DZE at $(Q, v') = (0, \infty)$; and numerical experiments indicate that with diminishing ε the Hopf bifurcation moves upwards along the curve, the branch of limit cycles shrinks, and the conjugate pair of pure imaginary eigenvalues that defines the Hopf bifurcation approaches zero. This scenario is sketched in Fig. 3 (in consideration of which it should be kept in mind that, conveniently, ε can be varied without changing the position of the steady states).

It would seem, therefore, that some essential physics is still missing from the model.

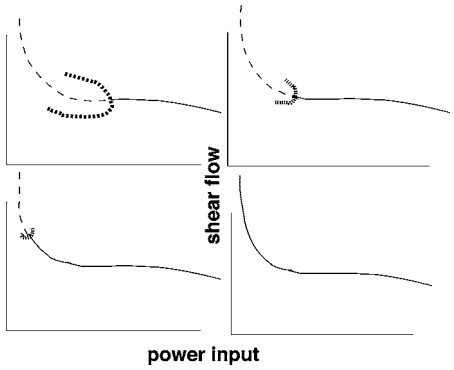

FIG. 3. Sketched snapshots, viewed from left to right, of the high shear flow branch in Fig. 2(b) as the thermal capacitance parameter ε is decreased.

B. A trapped singularity is found

What is not shown in Fig. 2 (because a log-scaled Q is used for illustrative purposes) is the branch of equilibria that exists at $Q=0$, where $N=0$ and $v' = (P^{3/2}\varphi)/b$; it is shown in Fig. 4(a). (In this and subsequent diagrams, where amplitude envelopes of oscillatory domains are not plotted for clarity, the Hopf bifurcations are annotated with the asterisks.) This branch might be considered trivial—except that there is a degenerate singularity on it, labeled as s4, where the zero and positive N branches intersect. The singularity s4 is described as "trapped" or persistent because it is not dissolved (or released or unfolded) by varying any of the parameters that are already present in the model (see Appendix B). This tells us that an additional term is required to achieve a smooth unfolding of s4, for which there must be some matching physics.

C. Shear flows also generate turbulence

The key to the release (or unfolding) of s4 lies in recognizing that kinetic energy in large-scale structures inevitably feeds the growth of turbulence at smaller scales, as well as vice versa.[2] In a flow, such as a magnetized plasma, where fluid elements locally experience a velocity field that is strongly two dimensional there will be a strong tendency for turbulent energy in the smaller scales to transfer to large-scale coherent structures such as shear flows (or an inverse energy cascade[1]), but the net rate of energy transfer to high wave numbers (or Kolmogorov cascade) is not negligible. A real-life flow experiences a three-dimensional velocity field in general, even though two-dimensional velocity fields can dominate locally. This fact is not reflected in Eqs. (4) and (5), and the derived low-order model, Eqs. (1)–(3), which describe an idealized flow under a purely two-dimensional velocity field. What is analogous to an ultraviolet catastrophe in the flow physics when energy transfer to high wave numbers is neglected maps to a trapped (or persistent) degenerate singularity in the mathematical structure of the model.

The trapped singularity s4 is unfolded smoothly by including a simple, conservative, back-transfer rate between the shear flow and turbulence subsystems:

$$\frac{dN}{dt} = \gamma NP - \alpha v'^2 N - \beta N^2 + \kappa v'^2, \tag{6}$$

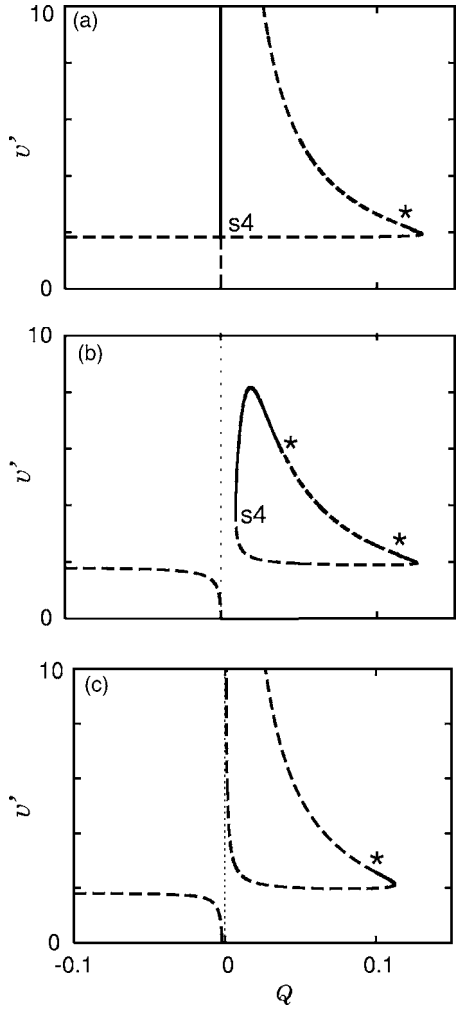

FIG. 4. (a) Equilibrium solutions of Eqs. (1)–(3) showing the branch at $Q=0$. (b) Equilibrium solutions of Eqs. (1), (6), and (7), for $\kappa=0.001$. (c) Equilibrium solutions of Eqs. (1), (8), and (3), for $c=0.005$. The values of the other parameters for all three bifurcation diagrams are $\varphi=0.08$, $b=1$, $\gamma=1$, $\varepsilon=1$, $\beta=0.3$, $a=0.3$, and $\alpha=2.4$.

$$2\frac{dv'}{dt} = \alpha v' N - \mu(P,N)v' + \varphi - \kappa v'. \tag{7}$$

The enhanced model consists of Eqs. (1), (6), and (7), and the corresponding energy flux diagram is shown in Fig. 5. At this stage the back-transfer rate coefficient κ need not be identified with any particular animal in the zoo of plasma and fluid instabilities, such as the Kelvin-Helmholtz instability; at this macroscopic level of modeling it may be treated as a lumped dimensionless parameter that provides a simple model for the overall physics of energy flux to high wave numbers.

The manner and consequences of unfolding s4 can be appreciated from Fig. 4(b). In comparing the structure of (a) and (b) one learns a salutary lesson: unphysical equilibria and singularities should not be ignored or dismissed as irrelevant, because they can play an important role in determining bifurcation structure in the physical domain.

The unfolding of s4 using a small positive value of κ in Fig. 4(b) necessarily creates a finite maximum in the shear flow, because s4 is a turning point, thus the unphysical situation of unbounded shear flow growth with decreasing power input is eliminated. At the given values of the other parameters the unfolding creates a finite-area isola (island) of steady-state solutions. (Isolas of steady-state solutions were first reported in the chemical engineering literature, where reduced dynamical models for reacting flows typically include a thermal or chemical autocatalytic reaction rate.[11]) Note also the appearance of another Hopf bifurcation on the isola in Fig. 4(b). The numerical evidence indicates that this Hopf bifurcation is trapped in another DZE at $(Q,v')=(0,\infty)$ in (a): both real and complex parts of a pair of complex-conjugate eigenvalues along this branch approach zero as $Q\to 0$.

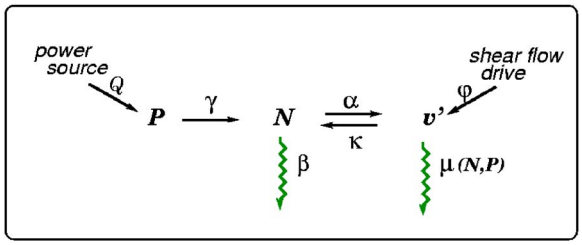

FIG. 5. The energy flux schematic now includes a channel for downscale transfer of energy from shear flow to turbulence subsystems.

The unfolding term $\kappa v'^2$ removes the zero-turbulence solution at zero power input. It says that even in the absence of gradient potential-energy conversion to turbulence and shear flow kinetic energy, some turbulence is generated because the effective direct shear flow drive φ is, in general, nonzero. In this case the long-term evolution of the system is simply

$$\frac{dN}{dt} = \kappa v'^2 - \beta N^2,$$

$$2\frac{dv'}{dt} = \varphi - \kappa v'.$$

The physical origin of energy transfer from the shear flow to turbulence may be thought of as a tertiary instability that increases monotonically with shear flow amplitude, and which, in general, may be sensitive to many factors such as magnetic shear, toroidal curvature, and background thermal gradients.[12] For the purpose of unfolding the degenerate singularity s4 the coefficient κ may be viewed as the first term of an expansion, in which second and higher terms (which need not be small) depend on the other factors, collectively designated ξ: $\kappa=\kappa_0+\kappa_1(\xi)+\cdots$. Since s4 is fully unfolded by $\kappa=\kappa_0$, the inclusion of further terms introduces *no* further qualitative changes local to s4.

One can suggest other possible candidates for a physics-based unfolding of s4. Indeed, the simplest perturbation that removes the degeneracy is a constant, external turbulence drive c, which recasts Eq. (2) as

$$\frac{dN}{dt} = \gamma NP - \alpha v'^2 N - \beta N^2 + c. \tag{8}$$

However, this unfolding on its own brings no improvement to the model because it fails to limit the growth of the shear flow. That is, it removes the turning point s4 itself, as well as the higher-order degeneracies, so that no shear flow maximum is created. The partial bifurcation diagram for Eqs. (1), (8), and (3) is given in Fig. 4(c). Thus the shear flow can still increase without bound as the power input is withdrawn, and we are no better off. The constant external turbulence drive c may certainly be included in Eq. (6), as well as the conservative energy-transfer rate $\kappa v'^2$, but it produces no additional qualitative effect on the bifurcation structure of the system.

It may also be proposed to unfold s4 by including new terms in the shear flow or potential-energy evolution equations. All such terms can be shown to be qualitatively ineffectual *locally* with respect to s4. For example, the term $-\kappa v'$ may be introduced into Eq. (3) only, purely as a dissipative channel:

$$2\frac{dv'}{dt} = \alpha v' N - [\mu(P,N) + \kappa]v' + \varphi.$$

It can be seen that this simply induces a quantitative shift in the hysteresis, exhibited in Fig. 2(a), that is due to dissipative loss of the shear flow.

If we now visualize the bifurcation diagram, with its *curves* of equilibrium solutions, as a slice of a three-dimensional *surface* of equilibrium solutions where the third coordinate is a second parameter, we can begin to understand the parameter space in perspective.

III. TWO SLICES REVEAL TWO DIFFERENT HYSTERESIS REGIMES

In Figs. 6 and 7 this surface of equilibria is sliced at $\varphi = 0.083$ and $\varphi = 0.084$, repectively, and in each figure (v', Q) (a) and (N, Q) (b) slices are shown. (A lower value of ε than that in Figs. 2 and 4 has been used so that the limit cycles onset and terminate at Hopf bifurcations, that is, form a stable oscillatory enclave rather than more exotic objects such as homoclinic terminii, which merely complicate the main issues explored here.) These two bifurcation diagrams illustrate the most dramatic physical consequence of unfolding the trapped singularity s4 and also suggest just a few of the operational regimes that may be possible. As in Fig. 2 the forward transition occurs at s1. Now, on what for obvious reasons is now designated as the *intermediate* branch, we let the power input ebb quasistatically.

In Fig. 6 the shear flow v' remains level (a) and the turbulence N declines (b) until the turning point s2 is reached, where the back-transition occurs. The isola, with its turning points s3 and s4 and small enclave of limit cycles can only be reached via a transient, either a nonquasistatic jump in a second parameter or evolution from initial conditions within the appropriate basin of attraction.

The dynamics is dramatically different in Fig. 7, where the isola has joined the "mainland" to form a peninsula (through the disappearance of s3 and s4 at a transcritical bifurcation, as mentioned in Sec. II). Around the neck of the peninsula, as the power input is withdrawn, the shear flow begins to grow (a) and the turbulence declines more steeply (b). The system transits through a domain of oscillatory solutions, where the turbulence and shear flow rise and fall out of phase, before emerging to a quiescent "supersuppressed" state. Along this segment the shear flow passes through a

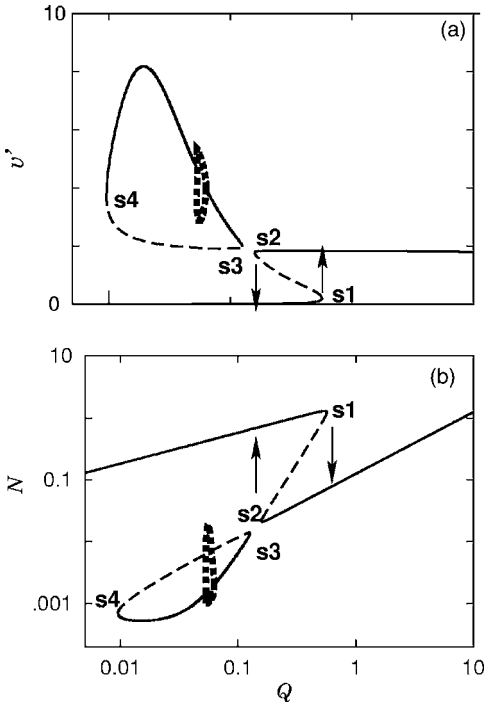

FIG. 6. The surface of equilibria is sliced at $\varphi = 0.083$. Other parameters $\varepsilon = 0.23$, $\kappa = 0.001$, $b = 1$, $\gamma = 1$, $\beta = 0.3$, $a = 0.3$, and $\alpha = 2.4$.

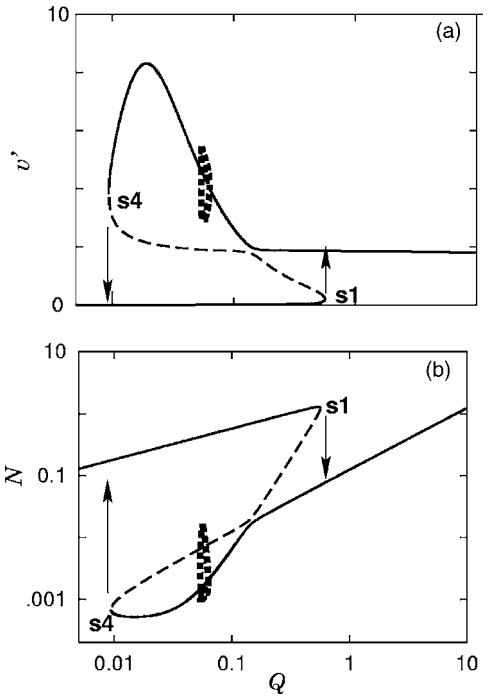

FIG. 7. The surface of equilibria is sliced at $\varphi = 0.084$. Other parameters $\varepsilon = 0.23$, $\kappa = 0.001$, $b = 1$, $\gamma = 1$, $\beta = 0.3$, $a = 0.3$, and $\alpha = 2.4$.

maximum then declines while the turbulence level reaches a minimum then rises a little. The back transition at s4 occurs at a very much lower power input than that at s2 in Fig. 6.

Even from just the two slices presented here we can see that there are many choices and tradeoffs to make in the design and operation of an experiment. Clearly the cost savings in terms of power input could be enormous if the system is transited at s1 then allowed to ride on the broad, deep hysteresis in the supersuppressed domain of Fig. 7. However, the limit cycles are not so well behaved if the thermal capacitance is much higher or the system is less efficiently dissipative: their behavior becomes three-dimensional with events such as period-doubling and torus bifurcations, and/or the branch can develop homoclinic terminii. On the other hand, in the well-behaved hysteresis loop of Fig. 6, which is less risky dynamically but more expensive to run in terms of power input, the improvement in confinement is not nearly so good.

IV. SUMMARY AND CONCLUSIONS

An enhanced dynamical model for confinement transitions that includes a simple rate term for downscale energy flux has been studied. The bifurcation structure shows that the shear flow can grow and pass through a maximum as the power input is withdrawn. The turbulence kinetic energy in this regime is supersuppressed.

The existence of the supersuppressed turbulence (or superenhanced shear flow) regime is due to a nonzero direct shear flow drive, modeled here as the simple nonspecific momentum input φ in Eq. (3). However, a model for downscale energy flux needs to be incorporated, giving Eqs. (6) and (7), to release the trapped turning point s4 (or back transition). This unfolding effectively prevents the shear flow becoming unbounded as power input is withdrawn; creating, instead, a shear flow maximum with corresponding turbulence minimum in the supersuppressed regime. In this regime the effect of the power input Q, which forces energy through the turbulence to large-scale shear flows via the Reynolds stress, and the effect of direct momentum injection to the shear flow via φ, reinforce each other.

The simulation and modeling results reported in Refs. 13 and 14 provide very good support for these results, because in those works a similar phenomenon was found using gyrokinetic equations for turbulence driven by the toroidal ion temperature gradient mode to derive a semiglobal model for the coupled dynamics of heat flux, fluctuation energy, and shear flow energy. The authors found that a suppressed-transport branch of solutions became more strongly suppressed as the perpendicular momentum deposition rate reinforced the Reynolds stress shear flow drive, and presented evidence that in the Japan Atomic Energy Research Institute Tokamak-60 Upgrade (JT-60U), the Princeton Beta eXperiment-Modified (PBX-M), and the Tokamak Fusion Test Reactor (TFTR) devices the signature of this branch is the emergence of the transport barrier in the core plasma.

For the analysis of the system modeled by Eqs. (1), (6), and (7) the control parameter is chosen as the power input Q, rather than the shear flow drive φ, since it is externally controllable by the experimenter whereas a lumped momentum input can have ungovernable internal components—friction with neutrals, for example.

In the supersuppressed turbulence (or superenhanced shear flow) peninsular domain of the parameter space of this model the dynamics is characterized by very broad hysteresis, a back transition at very low power input, and a region of oscillatory behavior.

For lower shear flow driving rates this peninsula of solutions is pinched off as an isola, and the "mainland" transition hysteresis is smaller, occurs at higher power input, and is well behaved or quiescent at low thermal capacitance but less effective in suppressing the turbulence.

This work provides the essential condition—a model for downscale energy flux—for the bifurcation stucture of the model to be mathematically smooth and correspondingly physically consistent. In forthcoming work other processes such as thermal diffusivity and ion orbit losses will be incorporated and their effects on the fundamental bifurcation structure as portrayed in Fig. 6 and 7 will be analyzed.

ACKNOWLEDGMENTS

I would like to thank W. Horton for bringing Refs. 13 and 14 to my notice. This work is supported by the Australian Research Council.

APPENDIX A: DEFINITION OF SYMBOLS AND NOTATION IN EQS. (4) and (5)

$\mathbf{v}=(1/B_0)\hat{\mathbf{z}}\times\nabla\phi=\mathbf{v}_0+\tilde{\mathbf{v}}$	$\mathbf{E}\times\mathbf{B}$ flow velocity
$\mathbf{v}_0=\langle\mathbf{v}\rangle$	Average background component
$\tilde{\mathbf{v}}$	Fluctuating or turbulent component
$p=p_0+\tilde{p}$	Plasma pressure
$p_0=\langle p\rangle$	Average background component
$\tilde{p}$	Fluctuating or turbulent component
B_0	Magnetic field along the z axis
ρ	Average mass density of ions, assumed constant
μ	Ion viscosity coefficient
η	Resistivity
ν	Frictional damping coefficient
$\Omega'\equiv d\Omega/dx>0$	Average field line curvature, assumed constant
$\nabla_\perp^2$	$\partial_x^2+\partial_y^2$
χ	Cross-field thermal diffusivity coefficient
V	External flow

APPENDIX B: A NOTE ON SINGULARITY THEORY METHODOLOGY AND TERMINOLOGY

This brief exposition on singularity and stability analysis follows Refs. 15 and 16, but relates it to the physical context of this work. A nontechnical reference accessible to the physics reader is Ref. 17, which also gives other key references on the mathematics and physical applications of singularity theory.

Systematic bifurcation, singularity, and stability analysis provide information on the global behavior of a dynamical system over its state and parameter space. It is qualitative information in the following sense.

In attempting to understand the behavior of a complex system with many degrees of freedom a standard approach is to begin by making a simplified model of the process—a dynamical system—and within the confines of that model analyze what it has to tell us about the process. Yet very few dynamical systems have exact solutions. For the vast majority it cannot even be proved that solutions exist, in general. The powerful methodologies of qualitative analysis, such as singularity and stability theories, can tell us how solutions *would* behave, assuming they *do* exist, as parameters are varied.

Although we may approximate solutions to finely detailed, spatially distributed dynamical systems on the computer, it is a formidable task to compute them over the entire parameter space. However, for an experimental or real-world macroscopic dynamical system we are often more interested in questions such as whether it is capable of discontinuous, periodic, or unstable behavior, and if so, what are the bounds of this behavior in parameter space so that we may design or manage our experiments to include, forbid, or modify such action. We can also use qualitative analysis to improve the model itself. In Appendix B 1 these capabilities of the singularity theory are illustrated using the model described by Eqs. (1)–(3).

1. Persistent, degenerate singularities inform us about physics

For a dynamical system

$$\frac{d\mathbf{x}}{dt} = \mathcal{F}(\mathbf{x}, \lambda_1, \ldots, \lambda_n), \tag{B1}$$

where the components of $\mathbf{x}$ are the dynamical state variables and the λ_i are the parameters, the equilibria are found by setting the right-hand sides to zero and solving to obtain a single algebraic equation in terms of one of the state variables x:

$$G(x, \lambda_1, \ldots, \lambda_n) = 0. \tag{B2}$$

The function $G(x, \lambda_1, \ldots, \lambda_n)$ is called the *bifurcation problem*. Solutions of (B2) that also satisfy the additional condition

$$G_x = 0, \tag{B3}$$

where the subscript notation denotes partial differentiation with respect to x, are called *singular* points or singularities. Points where conditions (B2) and (B3) hold and, in addition, one or more higher-order partial derivatives that are zero are known as *degenerate* or *higher-order* singularities.

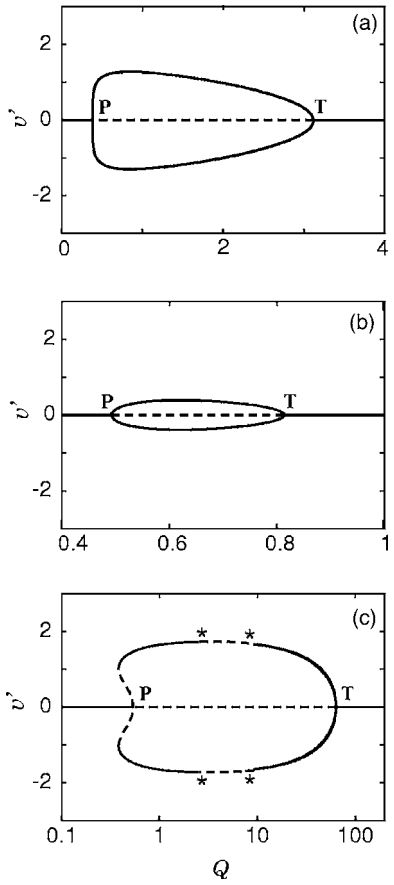

FIG. 8. Bifurcation diagrams showing the fully degenerate (a) and partially unfolded (b) and (c) pitchfork **P**. (a) $\beta=\beta_{\text{crit}}\approx 18.58$, (b) $\beta=50$, and (c) $\beta=1$. Other parameters $\varphi=0$, $\gamma=1$, $b=1$, $a=0.3$, $\alpha=2.4$, and $\varepsilon=1.5$.

An example of a degenerate singularity that has physical importance in the current context is the pitchfork, for which the defining and nondegeneracy conditions are

$$G = G_x = G_{xx} = G_{\lambda_1} = 0, \quad G_{xxx} \neq 0, \quad G_{x\lambda_1} \neq 0. \tag{B4}$$

Applying these conditions to Eqs. (1)–(3) we find, with the aid of some computer algebra, the unique pitchfork **P** at

$$(v', Q, \beta, \varphi) = \left(0, \frac{\alpha^2\gamma^2}{9a^2b}, \frac{2\alpha^3\gamma\sqrt{\alpha/a}}{27\sqrt{3}a^2b}, 0\right). \tag{P}$$

At **P** the two nondegeneracy conditions in Eq. (B4) evaluate as $g_{PQ}=8a/\alpha$ and $g_{PPP}=-18a\gamma^2/(\alpha\beta)$. We see that the pitchfork is a twice degenerate, or codimension 2, singularity because two parameters in addition to the principal bifurcation parameter Q are required to define it. The bifurcation diagram for the equilibria of Eqs. (1)–(3) at the critical values of the dissipative parameter β and the symmetry-breaking parameter φ is shown in in Fig. 8(a). In (b) and (c) β is relaxed a either side of the critical value, but φ is held at zero.

The other singularity **T** on $v'=0$ in Fig. 8 satisfies the defining and nondegeneracy conditions for a transcritical bifurcation,

$$G = G_x = G_{\lambda_1} = 0,$$

$$G_{xx} \neq 0, \quad \det\begin{pmatrix} G_{xx} & G_{\lambda_1 x} \\ G_{x\lambda_1} & G_{\lambda_1\lambda_1} \end{pmatrix} \equiv \det d^2G < 0. \tag{B5}$$

It is once degenerate but also requires the symmetry-breaking parameter for full determination.

We see from Fig. 8 that the pitchfork is persistent to variations in β. (In fact, it is persistent to variations in all parameters of Eqs. (1)–(3) other than φ. Persistence of a degenerate singularity when there are not enough independent parameters to unfold it was not recognized in some previous models for confinement transitions, where such points were wrongly claimed to represent second-order phase transitions.) Furthermore, as long as the degenerate singularity **P** persists the model cannot be predictive near it. This may be viewed as an overdetermination problem: with φ fixed at zero we see from (B4) there are four defining conditions but we have only three variable quantities, v', Q, and β.

Typically the pitchfork is associated with a fragile symmetry in the physics of the modeled system. In this case the symmetry is obvious from Fig. 8: in principle the shear flow can be in either direction equally. In real life (or *in numero*), experiments are always subject to perturbations that determine a preferred direction for the shear flow (such as friction with neutrals, or any other asymmetric shear-inducing mechanism), and the pitchfork is inevitably dissolved, or unfolded. In the bifurcation diagrams of Figs. 2, 4, 6, and 7 the pitchfork in Fig. 8 is fully unfolded, giving us a more realistic picture of confinement transition dynamics.

A third example of a degenerate singularity in this work is s4, in Fig. 4(a) and discussed in Sec. II C. s4 in Fig. 4(a) may be classified as an infinitely degenerate turning point. The defining conditions for a turning point (also called a saddle-node bifurcation, or sometimes a blue sky bifurcation) are

$$G = G_x = 0, \quad G_{xx} \neq 0, \quad G_{\lambda_1} \neq 0. \tag{B6}$$

For the zero-turbulence equilibrium solution of Eqs. (1)–(3) at $Q=0$ we can see by inspection that one or both of the nondegeneracy conditions in (B6) fail. The conditions (B6) may also be applied to the equilibria of Eqs. (1), (6), and (7), to check the classification of the unfolded s4. Since the resulting algebraic expressions are extremely long in this case it is neither interesting nor appropriate to reproduce them here, but the result can be reproduced easily using a computer algebra package. Briefly, one solves the zeros of Eqs. (1) and (6) for P and N, which are substituted in Eq. (7) to obtain the bifurcation equation $G(v')$. After obtaining the partial derivatives $G_{v'}$, $G_{v'v'}$, and G_Q, the system $G=G_{v'}=0$ may be solved in terms of φ and b. This invokes the implicit function theorem to parametrize the system using v'. Substituting the expressions for φ and b into $G_{v'v'}$ and G_Q completes the verification of conditions (B6) at s4.

In general when analyzing a dynamical model we are interested in the mapping between the bifurcation and stability structure and the physics of the process the model is supposed to represent. If we probe this relationship we find that degenerate singularities correspond to some essential physics (such as fulfilling a symmetry-breaking imperative, or the onset of hysteresis, or resolving an "ultraviolet catastrophe" type of anomaly), or they are pathological. In the first case we can usually unfold the singularity in a physically meaningful way; in the other case we know that something is amiss and we should revise our assumptions.

[1] R. H. Kraichnan and D. Montgomery, Rep. Prog. Phys. **43**, 547 (1980).
[2] P. W. Terry, Rev. Mod. Phys. **72**, 109 (2000).
[3] R. Ball, R. L. Dewar, and H. Sugama, Phys. Rev. E **66**, 066408 (2002).
[4] H. R. Strauss, Phys. Fluids **20**, 1354 (1977).
[5] B. A. Carreras, L. Garcia, and P. H. Diamond, Phys. Fluids **30**, 1388 (1987).
[6] H. Sugama and M. Wakatani, J. Phys. Soc. Jpn. **57**, 2010 (1988).
[7] H. Sugama and W. Horton, Phys. Plasmas **1**, 345 (1994).
[8] H. Sugama and W. Horton, Phys. Plasmas **1**, 2220 (1994).
[9] H. Sugama and W. Horton, Plasma Phys. Controlled Fusion **37**, 345 (1995).
[10] R. Ball and R. L. Dewar, Phys. Rev. Lett. **84**, 3077 (2000).
[11] R. Ball, Proc. R. Soc. London, Ser. A **455**, 141 (1999).
[12] B. N. Rogers, W. Dorland, and M. Kotschenreuther, Phys. Rev. Lett. **85**, 5336 (2000).
[13] Y. Kishimoto, T. Tajima, M. LeBrun, W. Horton, J.-Y. Kim, J. Dong, F. Waelbroeck, S. Tokuda, M. Kawanobe, and T. Fukuda, Plasma Phys. Controlled Nucl. Fusion Res. **3**, 299 (1994).
[14] W. Horton, T. Tajima, J.-Q. Dong, Y. Kishimoto, and J.-Y. Kim, Comments Plasma Phys. Controlled Fusion **17**, 205 (1996).
[15] M. Golubitsky and D. G. Schaeffer, *Singularities and Groups in Bifurcation Theory* (Springer, New York, 1985), Vol. 1.
[16] V. I. Arnold, *Mathematical Methods of Classical Mechanics*, translated by K. Vogtmann and A. Weinstein (Springer, New York, 1978).
[17] R. Ball, in *Encyclopedia of Nolinear Science*, edited by A. Scott (Taylor & Francis, New York, 2005).